Inorganic Chemistry

ARTICLE

pubs.acs.org/IC

Redox Chemistry, Acid Reactivity, and Hydrogenation Reactions of Two-Electron Mixed Valence Diiridium and Dirhodium Complexes

Thomas S. Teets, Timothy R. Cook, Brian D. McCarthy, and Daniel G. Nocera*

Department of Chemistry, 6-335, Massachusetts Institute of Technology, 77 Massachusetts Avenue, Cambridge, Massachusetts 02139-4307, United States

Supporting Information

ABSTRACT: The syntheses and reaction chemistry of two electron mixed-valence diphosphazane-bridged dirhodium and diiridium complexes $M_2^{0,II}(tfepma)_2(CN^tBu)_2Cl_2$ [M = Rh (**1**), Ir (**2**); tfepma = $MeN[P(OCH_2CF_3)_2]_2$, CN^tBu = *tert*-butyl isocyanide] are described. **1** and **2** undergo addition and two-electron oxidation and reduction chemistries. In the presence of CN^tBu, the addition product with the stoichiometry $M_2^{0,II}(tfepma)_2(CN^tBu)_3Cl_2$ [M = Rh (**3**), Ir (**3**)] is generated; in the presence of 1 equiv of CN^tBu and 2 equiv of bis(pentamethyl-cyclopentadienyl)cobalt(II), **1** and **2** are reduced to furnish $M_2^{0,0}(tfepma)_2(CN^tBu)_3$ [M = Rh (**5**), Ir (**6**)], which feature both four- and five-coordinate M^0 centers. Complexes **1**, **2**, **5**, and **6** all possess coordinatively unsaturated square planar M^0 centers that are reactive: (1) **2** reacts with $PhICl_2$ to produce $Ir_2^{II,II}(tfepma)_2(CN^tBu)_2Cl_4$ (**7**); (2) protonation of **2** with HX yields $Ir_2^{II,II}(tfepma)_2(CN^tBu)_2Cl_2HX$ [X = Cl^- (**8**), OTs^- (**9**)]; (3) protonation of **5** with HOTs produces $[Rh_2^{I,I}(tfepma)_2(CN^tBu)_3(\mu\text{-}H)](OTs)$; and (4) the reversible hydrogenation of **2** proceeds smoothly, furnishing the cis-dihydride complex $Ir_2^{II,II}(tfepma)_2(CN^tBu)_2(H)_2Cl_2$ (**11**). Substitution of tfepma in **2** with bis(diphenylphsophino)methane (dppm) yields the orthometalated complex $Ir_2^{II,II}(dppm)(PPh(o\text{-}C_6H_4)CH_2PPh_2)(CN^tBu)_2Cl_2H$ (**12**). The X-ray crystal structures of 11 compounds are presented and discussed, and spectroscopic characterization by multinuclear and variable temperature NMR provides details about solution structures and in some cases the formation of isomeric products. The electronic spectra of the new complexes are also described briefly, with absorption and emission features derived from the bimetallic core.

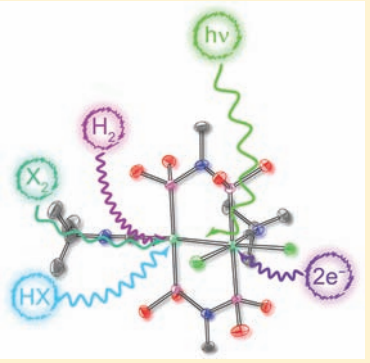

INTRODUCTION

Solar energy storage is arguably one of the most important factors governing the widespread deployment of solar energy resources.[1] The splitting of acid halides (HX, X = Cl, Br) into H_2 and X_2 is an energetically uphill reaction, which, when executed photocatalytically, can store quantities of solar energy comparable to that of the much heralded water-splitting reaction.[2] Bimetallic complexes are especially adept at catalyzing the two-electron, two-proton HX splitting photoreaction. Early success was realized with diphosphazane-bridged dirhodium complexes of the type $Rh_2^{0,0}(dfpma)_3L_2$ (dfpma = bis(difluorophosphino)methylamine, L = CO, PR_3), which photocatalyze hydrogen production from HX[3] via dihydride-dihalide $Rh_2^{II,II}$ intermediates.[4]

The two half-reactions of HX splitting, formally the reduction of protons to H_2 and the oxidation of halides to X_2, each present their own unique set of challenges, which must be simultaneously overcome to design more efficient photocatalysts. Our interrogation of the dirhodium catalysts affirmed that the sluggish halogen photoelimination limited the overall catalytic efficiency,[5,6] motivating the study of more efficient halogen elimination from bimetallic and monometallic centers.[7−11] The reductive half-reaction of HX splitting proceeds through hydrido-halide intermediates, generated by oxidative addition of HX. In previous work, HX addition was found to be preceded by photochemical CO liberation from a five-coordinate Rh^0 center, generating a reactive four-coordinate center.[3] This necessity to photoactivate the metal prior to HX addition translates to hydride-containing intermediates present in only minor quantities, and often these types of intermediates are unstable under the conditions used to generate them. Accordingly, these limitations obviate the structural and spectral characterization of key hydride intermediates of the catalytic cycle.

By avoiding high coordination metal centers, key hydride intermediates may be generated by thermal addition of HX and H_2 to group 9 two-electron mixed valence complexes that feature coordinatively unsaturated M^0 centers. In addition to allowing the thorough characterization of ground and excited state reactivity as it pertains to HX splitting, the late transition metal hydride complexes are of potential interest to those studying hydrogenation,[12] O_2 reduction,[13] aerobic oxidation,[14−17] and CO_2 reduction chemistries,[18] among others.[19] Indeed, we have shown that by using only two bridging diphosphazane ligands and a sufficiently bulky monodentate ligand, *tert*-butyl isocyanide, the complex $Rh_2^{0,II}(tfepma)_2(CN^tBu)_2Cl_2$ (**1**) could be accessed, and it reacts rapidly with HCl to generate a hydrido-chloride complex which shows interesting O_2-reduction reactivity.[20] Here, we expand the chemistry of **1** as well as the rich reaction chemistry

Received: March 14, 2011
Published: May 10, 2011

associated with the diiridium congener $Ir_2^{0,II}(tfepma)_2(CN^tBu)_2Cl_2$ (**2**) by describing two electron reduction and oxidation transformations. Bimetallic hydride complexes are obtained by protonation and hydrogenation of **2**. The results described herein provide access to a new suite of dirhodium and diiridium hydride complexes, which are promising targets to further our understanding of both H_2 production and O_2 reduction mediated by group 9 bimetallic complexes.

EXPERIMENTAL SECTION

General Considerations. All reactions involving air-sensitive materials were executed in a nitrogen-filled glovebox or on a high-vacuum manifold using solvents previously dried by passage through an alumina column under argon. The starting materials $[Ir^I(COD)Cl]_2$ (COD = 1,5-cyclooctadiene) and bis(diphenylphosphino)methane (dppm) were obtained from Strem Chemicals. 2,6-lutidine, HCl (1 M in Et_2O), bis(pentamethylcyclopentadienyl)cobalt(II) ($CoCp^*_2$), *p*-toluenesulfonic acid hydrate ($HOTs \cdot H_2O$), and *tert*-butylisocyanide (CN^tBu) were obtained from Sigma-Aldrich, whereas H_2 was purchased from Airgas. Anhydrous 2,6-lutidinium hydrochloride ($LutH^+Cl^-$) was prepared by adding anhydrous 2,6-lutidine to 1 M HCl/Et_2O under nitrogen. The ligand bis(bis(trifluoroethoxy)phosphino)methylamine (tfepma),[21] $PhICl_2$[22] and $Rh_2^{0,II}(tfepma)_2(CN^tBu)_2Cl_2$[20] were prepared as described in the literature. Elemental analyses were performed by Midwest Microlab LLC or Quantitative Technologies Incorporated.

Physical Methods. NMR spectra were recorded at the MIT Department of Chemistry Instrumentation Facility on a Varian Mercury 300 NMR Spectrometer or a Varian Inova-500 NMR Spectrometer. $^{31}P\{^1H\}$ NMR spectra were referenced to an external standard of 85% D_3PO_4, and ^1H spectra were referenced to the residual proteo solvent resonances. UV−vis samples were prepared in a nitrogen-filled glovebox, and spectra were recorded at 293 K in tetrahydrofuran (THF) solutions in quartz cuvettes on a Varian Cary 5000 UV−vis−NIR spectrophotometer. Extinction coefficients were determined over a concentration range of $\sim 10^{-6}-10^{-4}$ M, for which all compounds obeyed Beer's Law. IR spectra were recorded on a PerkinElmer Spectrum 400 FT-IR/FT-FIR Spectrometer outfitted with a Pike Technologies GladiATR attenuated total reflectance accessory with a monolithic diamond crystal stage and pressure clamp. Samples were suspended in Nujol mineral oil for all IR measurements. Steady state emission spectra were recorded on an automated Photon Technology International (PTI) QM 4 fluorimeter equipped with a 150-W Xe arc lamp and a Hamamatsu R928 photomultiplier tube. Excitation light was excluded with appropriate glass filters. Samples were housed in custom quartz EPR tubes with a ground-glass joint and Teflon plug. Solution samples were prepared in 2-methyltetrahydrofuran and freeze pump thaw degassed (4 cycles, 1×10^{-5} Torr). The sample tubes were immersed in liquid N_2 in a quartz finger dewar prior to measurement.

Preparation of $Ir_2^{0,II}(tfepma)_2(CN^tBu)_2Cl_2$ (2). $[Ir^I(COD)Cl]_2$ (421 mg, 0.627 mmol, 1.00 equiv) was suspended in 3 mL of Et_2O in a 20-mL scintillation vial. A solution of tfepma (611 mg, 1.25 mmol, 2.00 equiv), dissolved in 2 mL of Et_2O, was added at a fast dropwise rate to give a dark yellow/brown solution. A solution of CN^tBu (104 mg, 1.25 mmol, 2.00 equiv) in 2 mL of Et_2O was added immediately, giving a dark red solution. The reaction mixture was stirred at room temperature for 22 h, during which time some orange solid had formed. The mixture was concentrated to dryness, leaving an orange solid and a red residue. The product was resuspended in 2 mL of Et_2O, and 16 mL of pentane was added to the stirred mixture, liberating a light orange solid. The supernatant was decanted, and the solid briefly dried in vacuo. The product was dissolved in 10 mL of CH_2Cl_2 and filtered, removing a small amount of a brown impurity. The solvent was removed in vacuo, and the resulting solid was resuspended in 1 mL of CH_2Cl_2/15 mL of pentane. The mixture was chilled overnight at −20 °C, at which time the supernatant was decanted and the light orange product dried in vacuo. Yield: 643 mg (64.3%). ^1H NMR (500 MHz, CD_2Cl_2) δ/ppm: 4.96−5.13 (m, 4H), 4.77−4.88 (m, 2H), 4.47−4.64 (m, 4H), 4.29−4.46 (m, 6H), 2.87 (pseudoquintet, 6H), 1.38 (s, 9H), 1.33 (s, 9H). $^{31}P\{^1H\}$ NMR (121.5 MHz, CD_2Cl_2) δ/ppm: 132.3 (m, 2P), 85.9 (m, 2P). UV−vis (CH_3CN): λ/nm (ε/M^{-1} cm^{-1}) 271 (15000), 315 (6300), 338 (sh) (4100), 392 (5600), 449 (1600), 504 (860). IR (Nujol): $\tilde{\nu}_{C\equiv N}$ = 2071 (sh), 2132 (sh), 2100 cm^{-1}. Anal. Calcd. for $C_{28}H_{40}Cl_2F_{24}N_4O_8P_4Ir_2$: C, 21.07; H, 2.53; N, 3.51. Found: C, 20.97; H, 2.49; N, 3.27.

Preparation of $[Rh_2^{0,II}(tfepma)_2(CN^tBu)_3Cl]Cl$ (3). To a solution of **1** (100 mg, 0.0706 mmol, 1.00 equiv) in 2 mL of THF was added a solution of CN^tBu (6.2 mg, 0.074 mmol, 1.1 equiv) in 0.5 mL of THF, causing the color to darken slightly. The reaction was stirred at room temperature for 2.5 h, following which the solvent was removed in vacuo. The residue was washed with 4 mL of Et_2O and 2 mL of hexane, leaving a yellow solid which was dried in vacuo. The product was dissolved in 1.5 mL of THF and layered with 15 mL of hexane to recrystallize. After about 48 h the supernatant was decanted, and the product dried in vacuo. Yield: 63 mg (59%). Repeated attempts to obtain analytically pure material by various recrystallization procedures were unsuccessful, likely because of the reversible nature of the reaction. ^1H NMR (500 MHz, CD_3CN) δ/ppm: 4.15−5.15 (m, 16H), 2.95 (br, s, 6H), 1.47 (br, s, 27H). $^{31}P\{^1H\}$ NMR (121.5 MHz, CD_3CN) δ/ppm: 144.0 (br, m, 2P), 125.7 (br, m, 2P). IR (Nujol): $\tilde{\nu}_{C\equiv N}$ = 2131, 2160 cm^{-1}. Anal. Calcd. for $C_{33}H_{49}Cl_2F_{24}N_5O_8P_4Rh_2$: C, 26.42; H, 3.29; N, 4.67. Found: C, 25.04; H, 3.17; N, 4.49.

Preparation of $Ir_2^{0,II}(tfepma)_2(CN^tBu)_3Cl_2$ (4). A sample of **2** (100 mg, 0.0627 mmol, 1.00 equiv) was dissolved in 1.5 mL of THF. A solution of CN^tBu (5.7 mg, 0.068 mmol, 1.1 equiv) in 0.5 mL of THF was added, and the yellow-orange solution was stirred at room temperature for 24 h. The solution was concentrated in vacuo to give a yellow-orange residue, which was suspended in 1 mL of CH_2Cl_2/15 mL of pentane and chilled at −20 °C for 24 h. The supernatant was decanted, and the resulting yellow product dried in vacuo. Yield: 73 mg (70%). Analytically pure material was obtained in much lower yields (<50%) by recrystallization from a concentrated CH_2Cl_2 solution layered with pentane. ^1H NMR (500 MHz, CD_3CN) δ/ppm: 4.86−4.97 (m, 4H), 4.44−4.69 (m, 12H), 2.94 (pseudoquintet, 6H), 1.45 (s, 9H), 1.43 (s, 18H). $^{31}P\{^1H\}$ NMR (121.5 MHz, CD_3CN) δ/ppm: 132.3 (m, 2P), 79.8 (m, 2P). UV−vis (CH_3CN): λ/nm (ε/M^{-1} cm^{-1}) 271 (16000), 307 (5300), 325 (sh) (3700), 382 (6400), 444 (1800), 496 (960). IR (Nujol): $\tilde{\nu}_{C\equiv N}$ = 2116, 2159, 2181 cm^{-1}. Anal. Calcd. for $C_{33}H_{49}Cl_2F_{24}N_5O_8P_4Ir_2$: C, 23.61; H, 2.94; N, 4.17. Found: C, 22.95; H, 2.85; N, 4.05.

Preparation of $Rh_2^{0,0}(tfepma)_2(CN^tBu)_3$ (5). A mixture of **1** (475 mg, 0.335 mmol, 1.00 equiv) and CN^tBu (27.9 mg, 0.336 mmol, 1.00 equiv) were dissolved in 6 mL of THF, giving a red-orange solution and a small amount of yellow precipitate. The mixture was added via pipet to a stirred solution of $CoCp^*_2$ (221 mg, 0.671 mmol, 2.00 equiv) in 2 mL of THF. Yellow $[CoCp^*_2]Cl$ formed immediately, and the mixture was allowed to stir at room temperature for 3 h. A yellow-green solid was removed by filtration through a plug of glass wool, and the volatiles were removed in vacuo to afford a dark red residue. The product was dissolved in a mixture of 2 mL of Et_2O/2 mL of hexanes, and upon concentrating in vacuo an orange solid was obtained. The solid was suspended in 8 mL of hexanes at −20 °C overnight. The supernatant was decanted, and the solid was dried in vacuo. Yield: 432 mg (90.2%). ^1H NMR (500 MHz, C_6D_6) δ/ppm: 4.13−4.40 (br, m, 16H), 2.80 (br, pseudoquintet, 6H), 1.04 (br, s, 27H). $^{31}P\{^1H\}$ NMR (121.5 MHz, C_6D_6) δ/ppm: 156.0 (m, 4P). UV−vis (THF): λ/nm (ε/M^{-1} cm^{-1}) 285 (19000), 379 (6200). IR (Nujol): $\tilde{\nu}_{C\equiv N}$ = 2042 (sh), 2074 (sh), 2098 cm^{-1}. Anal. Calcd. for $C_{33}H_{49}F_{24}N_5O_8P_4Rh_2$: C, 27.73; H, 3.46; N, 4.90. Found: C, 27.80; H, 3.37; N, 4.80.

dx.doi.org/10.1021/ic2005248 |*Inorg. Chem.* 2011, 50, 5223–5233

Preparation of $Ir_2^{0,0}$(tfepma)$_2$(CN^tBu)$_3$ (6). A suspension of **2** (500 mg, 0.313 mmol, 1.00 equiv) in 6 mL of Et_2O was combined with a solution of CN^tBu (26.0 mg, 0.313 mmol, 1.00 equiv) in 2 mL of Et_2O. Most of the solid was drawn into solution, with only a small amount of undissolved orange solid remaining. The mixture was added to $CoCp^*_2$ (206 mg, 0.627 mmol, 2.00 equiv) in 2 mL of Et_2O. A yellow solid formed immediately, and the mixture was stirred for 3 h, at which time the precipitate was removed by filtration through glass wool and the solution concentrated to dryness. The resulting orange solid was suspended in 6 mL of pentane at −20 °C overnight. The supernatant was decanted, and the bright orange solid dried in vacuo. Yield: 410 mg (81.3%). ^{1}H NMR (500 MHz, C_6D_6) δ/ppm: 4.15−4.39 (br, m, 16H), 2.74 (pseudoquintet, 6H), 1.03 (s, 27H). $^{31}P\{^1H\}$ NMR (202.5 MHz, C_6D_6) δ/ppm: 126.1 (s, 4P). UV−vis (THF): λ/nm (ε/M^{-1} cm^{-1}) 266 (sh) (16000), 383 (4300). IR (Nujol): $\tilde{\nu}_{C\equiv N}$ = 2038 (sh), 2088 (sh), 2113 cm^{-1}. Anal. Calcd. for $C_{33}H_{49}F_{24}N_5O_8P_4Ir_2$: C, 24.65; H, 3.07; N, 4.36. Found: C, 24.72; H, 3.14; N, 4.27.

Preparation of $Ir_2^{II,II}$(tfepma)$_2$(CN^tBu)$_2$$Cl_4$ (7). In a 20-mL scintillation vial, **2** (100 mg, 0.0627 mmol, 1.00 equiv) was dissolved in 2 mL of CH_2Cl_2. In a separate vial, $PhICl_2$ (19.0 mg, 0.0691 mmol, 1.10 equiv) was dissolved in 2 mL of CH_2Cl_2. Both solutions were frozen in the glovebox coldwell. They were removed, and upon thawing the $PhICl_2$ solution was added dropwise to the solution of **1**. The color immediately lightened to canary yellow, and the reaction was allowed to warm to room temperature and stirred for 1 h. The resulting solution was concentrated in vacuo and triturated with 4 mL of hexane to yield a bright yellow solid. The product was washed with 2 mL of hexane and dried in vacuo. Yield: 90 mg (86%). ^{1}H NMR (500 MHz, CD_3CN) δ/ppm: 5.34−5.45 (m, 2H), 5.00−5.11 (m, 2H), 4.55−4.93 (m, 12H), 2.90 (pseudoquintet, 6H), 1.61 (s, 9H), 1.38 (s, 9H). $^{31}P\{^1H\}$ NMR (121.5 MHz, CD_3CN) δ/ppm: 76.1−77.6 (m, 2P), 70.3−71.8 (m, 2P) (AA′BB′, 12 lines resolved, δ_{avg} = 73.9 ppm) . UV−vis (CH_3CN): λ/nm (ε/M^{-1} cm^{-1}) 282 (18000), 333 (6200), 364 (sh) (2500). IR (Nujol): $\tilde{\nu}_{C\equiv N}$ = 2186 cm^{-1}. Anal. Calcd. for $C_{28}H_{40}Cl_4F_{24}N_4O_8P_4Ir_2$: C, 20.18; H, 2.42; N, 3.36. Found: C, 20.37; H, 2.41; N, 3.35.

Preparation of $Ir_2^{II,II}$(tfepma)$_2$(CN^tBu)$_2$$Cl_3H$ (8). In a 20-mL scintillation vial, **2** (100 mg, 0.0627 mmol, 1.00 equiv) was dissolved in 2 mL of acetonitrile. A solution of $LutH^+Cl^-$ (11.2 mg, 0.0780 mmol, 1.24 equiv) in 1 mL of acetonitrile was added, causing the color to fade to pale yellow. The solution was stirred at room temperature for 30 min, and then the solvent was removed in vacuo to give a cream-colored solid. The solid was taken up in 8 mL of Et_2O and filtered through a plug of glass wool to remove unreacted $LutH^+Cl^-$. To the resulting solution was added 2 mL of hexane, and concentration in vacuo left a light yellow solid, which was suspended in hexane and stored at −20 °C overnight. The supernatant was decanted, and the product dried in vacuo. Yield: 98 mg (96%). ^{1}H NMR (500 MHz, C_6D_6) δ/ppm: 5.93 (m, 2H), 5.62 (m, 2H), 5.44 (m, 2H), 4.96 (m, 2H), 4.80 (m, 2H), 4.64 (m, 2H), 3.93 (m, 4H), 2.54 (pseudoquintet, 6H), 1.08 (s, 9H), 1.03 (s, 9H), −20.69 (t, $^2J_{H-P}$ = 16.0 Hz, 1H). $^{31}P\{^1H\}$ NMR (121.5 MHz, C_6D_6) δ/ppm: 89.0−91.5 (m, 2P), 77.8−80.3 (m, 2P) (AA′BB′, 20 lines resolved, δ_{avg} = 84.7 ppm). UV−vis (THF): λ/nm (ε/M^{-1} cm^{-1}) 285 (12000), 322 (8300), 360 (sh) (2400). IR (Nujol): $\tilde{\nu}_{C\equiv N}$ = 2170 cm^{-1}. Anal. Calcd. for $C_{28}H_{41}Cl_3F_{24}N_4O_8P_4Ir_2$: C, 20.60; H, 2.53; N, 3.43. Found: C, 21.29; H, 2.31; N, 3.28.

Preparation of $Ir_2^{II,II}$(tfepma)$_2$(CN^tBu)$_2$$Cl_2H$(OTs) (9). In the glovebox, **2** (100 mg, 0.0627 mmol, 1.00 equiv) was dissolved in 2 mL of THF. A solution of HOTs·H_2O (12.5 mg, 0.0657 mmol, 1.05 equiv) in 1 mL of THF was added, giving a nearly colorless solution. After 48 h, the solvent was removed in vacuo. The product was redissolved in 4 mL of hexane/6 mL of Et_2O, and the resulting solution was concentrated in vacuo to leave a white solid, which was treated with 4 mL of hexane and stored at −20 °C overnight. The supernatant was decanted, and the product dried in vacuo. Yield: 104 mg (93.7%). Major isomer (89%): ^{1}H NMR (500 MHz, CD_3CN) δ/ppm: 7.60 (d, $^3J_{H-H}$ = 8.5 Hz, 2H), 7.16 (d, $^3J_{H-H}$ = 8.5 Hz, 2H), 5.23 (m, 2H), 4.60−5.00 (m, 10H), 4.37−4.45 (m, 4H), 2.92 (pseudoquintet, 6H), 2.33 (s, 3H), 1.55 (s, 9H), 1.43 (s, 9H), −20.00 (t, $^2J_{H-P}$ = 16.0 Hz, 1H). $^{31}P\{^1H\}$ NMR (121.5 MHz, CD_3CN) δ/ppm: 91.1−93.9 (m, 2P), 77.7−80.5 (m, 2P) (AA′BB′, 18 lines resolved, δ_{avg} = 85.8 ppm). Minor isomer (11%): ^{1}H NMR (500 MHz, CD_3CN) δ/ppm: 7.60 (d, $^3J_{H-H}$ = 8.5 Hz, 2H) (coincident with major isomer), 7.16 (d, $^3J_{H-H}$ = 8.5 Hz, 2H) (coincident with major isomer), 4.28−5.12 (m, 16H) (overlap with peaks from major isomer), 2.98 (pseudoquintet, 6H), 2.33 (s, 3H) (coincident with major isomer), 1.56 (s, 9H), 1.44 (s, 9H), −20.71 (t, $^2J_{H-P}$ = 16.0 Hz, 1H) $^{31}P\{^1H\}$ NMR (121.5 MHz, CD_3CN) δ/ppm: ∼92.7 (m, 2P), ∼78.9 (m, 2P). (peaks are completely overlapped with those of major isomer) UV−vis (CH_3CN) (mixture of isomers): λ/nm (ε/M^{-1} cm^{-1}) 270 (17000), 320 (5300), 348 (3500). IR (Nujol) (mixture of isomers): $\tilde{\nu}_{C\equiv N}$ = 2171, 2181 (sh), 2189 (sh) cm^{-1}. Anal. Calcd. for $C_{35}H_{48}Cl_2F_{24}N_4O_{11}P_4SIr_2$: C, 23.78; H, 2.74; N, 3.17. Found: C, 24.15; H, 2.42; N, 3.05.

Preparation of [$Rh_2^{I,I}$(tfepma)$_2$(CN^tBu)$_3$(μ-H)](OTs) (10). Separate solutions of **5** (100 mg, 0.0700 mmol, 1.00 equiv) in 2 mL of CH_3CN and HOTs·H_2O (13.3 mg, 0.699 mmol, 0.999 equiv) in 1 mL of CH_3CN were prepared and frozen in the glovebox coldwell. The solutions were removed, and upon thawing the HOTs solution was added dropwise to the stirred solution of **5**, giving a red-orange solution, which was allowed to warm to room temperature and stirred for 1 h. The solution was concentrated to dryness in vacuo, yielding a red residue. Trituration with 2 mL of Et_2O afforded a yellow solid, and the resulting suspension was placed in the freezer at −20 °C overnight. The product was isolated by decantation and dried in vacuo. Yield: 92 mg (82%). ^{1}H NMR (500 MHz, CD_3CN) δ/ppm: 7.59 (d, $^2J_{H-H}$ = 8.0 Hz, 2H), 7.14 (d, $^2J_{H-H}$ = 8.0 Hz, 2H), 4.28−4.50 (br, m, 16H), 2.80 (pseudoquintet, 6H), 2.32 (s, 3H), 1.45 (s, 27H), −12.63 (tquint, $^1J_{H-Rh}$ = 14.8 Hz, $^2J_{H-P}$ = 8.5 Hz, 1H). $^{31}P\{^1H\}$ NMR (121.5 MHz, CD_3CN) δ/ppm: 150.7 (m, 4P). UV−vis (CH_3CN): λ/nm (ε/M^{-1} cm^{-1}) 270 (13000), 283 (sh) (12000), 339 (sh) (4400), 376 (sh) (3900), 443 (sh) (1400). IR (Nujol): $\tilde{\nu}_{C\equiv N}$ = 2135, 2164 cm^{-1}. Anal. Calcd. for $C_{40}H_{57}F_{24}N_5O_{11}P_4SRh_2$: C, 30.00; H, 3.59; N, 4.37. Found: C, 29.65; H, 3.31; N, 4.27.

Preparation of $Ir_2^{II,II}$(tfepma)$_2$(CN^tBu)$_2$$Cl_2(H)_2$ (11). A J. Young NMR tube was charged with **2** (25 mg, 0.016 mmol) dissolved in 0.7 mL of THF-d_8. The solution was freeze−pump−thaw degassed three times on a high vacuum manifold. The tube was pressurized with about 1.5 atm of H_2 and upon shaking the tube a nearly colorless solution was obtained. The NMR spectra were immediately recorded. The compound is unstable in the absence of H_2, losing H_2 and reverting back to **2**. This instability precluded isolation of solid material for microanalysis. Crystals for X-ray diffraction and IR analysis were obtained by conducting an analogous preparation in CD_3CN and chilling the solution to −20 °C overnight in the presence of H_2. For the UV−vis measurement, a solution of **2** (63 μM in THF) was prepared in a septum-sealed cuvette, and 2 mL of H_2 was injected via gastight syringe. Major isomer (*cis*-H_2, *cis*-P_2): Yield (from NMR): 95%. ^{1}H NMR (500 MHz, THF-d_8) δ/ppm: 5.60 (m, 2H), 4.84 (m, 2H), 4.68 (m, 4H), 4.42−4.56 (m, 4H), 4.29 (m, 2H), 4.13 (m, 2H), 2.82 (m, 6H), 1.48 (s, 9H), 1.46 (s, 9H), −12.63 to −12.03 (m, 2H). $^{31}P\{^1H\}$ NMR (121.5 MHz, THF-d_8) δ/ppm: 93.4−97.8 (m, 2P), 88.2−90.4 (m, 2P). IR (Nujol): $\tilde{\nu}_{Ir-H}$ = 2036, 2065 cm^{-1}, $\tilde{\nu}_{C\equiv N}$ = 2161 cm^{-1}. Minor isomer (*cis*-H_2, *trans*-P_2): Yield (from NMR): 5%. ^{1}H NMR (500 MHz, THF-d_8) δ/ppm: 5.26 (m, 2H), 5.13 (m, 4H), about 4.84 (m, 2H) (overlap with major isomer), about 4.68 (m, 4H) (overlap with major isomer), 4.39 (m, 4H), 2.86 (pseudoquintet, 6H), 1.44 (s, 9H), 1.41 (s, 9H), −14.80 (td, $^2J_{H-P}$ = 17.9 Hz, $^2J_{H-H}$ = 4.6 Hz, 1H) −15.50 (td, $^2J_{H-P}$ = 13.8 Hz, $^2J_{H-H}$ = 4.6 Hz, 1H). $^{31}P\{^1H\}$ NMR (121.5 MHz, THF-d_8) δ/ppm: 109.6 (m, 2P), about 95.0 (m, 2P), (overlap with major isomer). UV−vis (THF) (both isomers present): λ/nm (ε/M^{-1} cm^{-1}) 267 (16000), 313 (4800), 342 (3300).

dx.doi.org/10.1021/ic2005248 |*Inorg. Chem.* 2011, 50, 5223–5233

Preparation of $Ir_2^{II,II}(dppm)(PPh(o\text{-}C_6H_4)CH_2PPh_2)(CN^tBu)_2Cl_2H$ (12). $[Ir^I(COD)Cl]_2$ (242 mg, 0.360 mmol, 1.00 equiv) was dissolved in 8 mL of THF to give an orange solution. A solution of dppm (276 mg, 0.718 mmol, 1.99 equiv) in 6 mL of THF was added, followed by CN^tBu (60 mg, 0.72 mmol, 2.0 equiv) in 6 mL of THF. The resulting dark green solution gradually faded to pale yellow, and over the course of 72 h stirring at room temperature a white solid precipitated from solution. The solid was collected by vacuum filtration, washed with 10 mL of THF and 10 mL of Et_2O and dried in vacuo. Yield: 374 mg (74.0%). ^1H NMR (500 MHz, CD_2Cl_2) δ/ppm: 8.02 (m, 2H), 7.89 (m, 4H), 7.64−7.71 (m, 3H), 7.48−7.58 (m, 3H), 7.34−7.44 (m, 3H), 7.15−7.25 (m, 7H), 6.93−7.12 (m, 10H), 6.72−6.81 (m, 4H), 6.59 (m, 1H), 6.51 (m, 2H), 4.69 (m, 1H), 4.47 (m, 1H), 4.39 (m, 1H), 3.86 (m, 1H), 1.09 (s, 9H), 0.73 (s, 9H), −10.69 (dd, $^2J_{H-P}$ = 163 Hz, 19.1 Hz, 1H). $^{31}P\{^1H\}$ NMR (121.5 MHz, CD_2Cl_2) δ/ppm: −9.8 to 1.5 (m, 2P), −20.7 to −19.6 (m, 1P), −33.4 (m, 1P). IR (Nujol): $\tilde{\nu}_{Ir-H}$ = 2097 cm^{-1}, $\tilde{\nu}_{C\equiv N}$ = 2134, 2162 cm^{-1}. Anal. Calcd. for $C_{60}H_{62}Cl_2N_2P_4Ir_2$: C, 51.83; H, 4.49; N, 2.01. Found: C, 51.76; H, 4.25; N, 2.02.

X-ray Crystallographic Details. Single crystals of **2**, **3**, and **4** were obtained by layering a CH_2Cl_2 solution with pentane, crystals of **5** and **6** were obtained from a toluene/pentane solution at −20 °C, crystals of **7** and **9** deposited from CH_2Cl_2/hexane at −20 °C, crystals of **8** were grown in Et_2O/pentane at −20 °C, crystals of **10** were obtained from THF/hexane at −20 °C, crystals of **11** were grown from a CD_3CN NMR sample at −20 °C, and crystals of **12** deposited from THF at room temperature. The crystals were mounted on a Bruker three circle goniometer platform equipped with an APEX detector. A graphite monochromator was employed for wavelength selection of the Mo Kα radiation (λ = 0.71073 Å). The data were processed and refined using the program SAINT supplied by Siemens Industrial Automation. Structures were solved by Patterson methods in SHELXS and refined by standard difference Fourier techniques in the SHELXTL program suite (6.10 v., Sheldrick G. M., and Siemens Industrial Automation, 2000). Hydrogen atoms bonded to carbon were placed in calculated positions using the standard riding model and refined isotropically; all non-hydrogen atoms were refined anisotropically. The metal-bound hydrogen atoms in **8**, **9**, **11**, and **12** were located in the difference map, restrained to a distance of 1.60 Å from the metal, and refined isotropically. The bridging hydride in **10** was restrained to be equidistant from the two rhodium nuclei. The crystal of **3** was a nonmerohedral twin; two unit cell domains were located using the program cell_now and used for integration in SAINT. The absorption correction was performed with TWINABS, and the structure was refined against the major twin component. The structures of **4**, **10**, and **12** all had one or more disordered $-OCH_2CF_3$ groups, and the structure of **7** had a disordered *tert*-butyl group. In addition, the structures of **4** and **9** also contained a disordered dichloromethane. The (1,2) and (1,3) distances of all disordered parts were restrained to be similar using the SADI command; the rigid-bond restraints SIMU and DELU were also used on disordered parts. Unit cell parameters, morphology, and solution statistics for the structures of **1**−**3** are summarized in Supporting Information, Tables S1−S3. All thermal ellipsoid plots are drawn with carbon-bound hydrogen atoms, solvent molecules and noncoordinating counterions omitted for clarity.

RESULTS

Synthesis and Characterization of $Ir_2^{0,II}(tfepma)_2(CN^tBu)_2Cl_2$ (2). We have previously reported the two-electron mixed valence complex $Rh_2^{0,II}(tfepma)_2(CN^tBu)_2Cl_2$ (**1**, tfepma = $[P(OCH_2CF_3)_2]_2NMe$), which contains an unsaturated four-coordinate Rh^0 center.[20] The diiridium counterpart, $Ir_2^{0,II}(tfepma)_2(CN^tBu)_2Cl_2$ (**2**), is prepared in nearly identical fashion, as described in Scheme 1. Treatment of $[Ir^I(COD)Cl]_2$ (COD = 1,5-cyclooctadiene) with stoichiometric amounts of tfepma and

Scheme 1

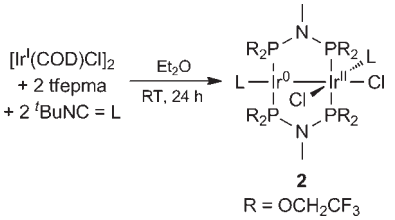

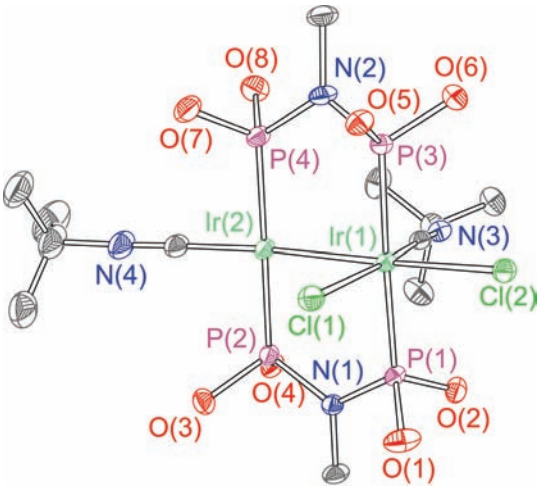

Figure 1. Thermal ellipsoid plot for **2**. Ellipsoids are shown at the 50% probability level with $-CH_2CF_3$ groups and hydrogen atoms omitted for clarity. Data were collected at 100 ± 2 K.

CN^tBu furnishes the two-electron mixed valence complex **2**, which was isolated in 64% yield after a 24 h reaction time. Spectroscopic characterization of **2** supports the formulation of a two-electron mixed valence core. In the ^1H NMR spectrum, two distinct *tert*-butyl resonances are observed at 1.38 and 1.33 ppm, suggesting chemical inequivalency of the two CN^tBu ligands owing to the mixed valence character of the bimetallic core. Furthermore, the $^{31}P\{^1H\}$ NMR spectrum (Supporting Information, Figure S1) shows two symmetric multiplets at 85.9 and 132.3 ppm, with characteristic multiplicities arising from the AA′XX′ spin system. In total, 16 of the possible 20 lines of the AA′XX′ splitting pattern are observed. Finally, the IR spectrum shows two distinct C≡N stretching frequencies at 2100 and 2132 cm^{-1}, once again indicative of an asymmetric structure for **2**.

X-ray crystallography confirms the two-electron mixed valence structure of diiridium complex **2**. As shown in Figure 1, distinct coordination environments are observed for the square planar, d^9 Ir^0 center and the octahedral, d^7 Ir^{II} center. The Ir(1)−Ir(2) internuclear distance of 2.7112(3) Å is consistent with a metal−metal bond, as expected for a d^7−d^9 complex. The bimetallic core is bridged by both tfepma ligands, as is the case for all complexes discussed here; there are no instances of chelating tfepma.

Reaction Chemistry. A reaction chemistry originating from **1** and **2** is summarized in Scheme 2. The chemical structures shown in Scheme 2 represent crystallographically confirmed geometries.

Addition of CN^tBu to 1 and 2. As **1** and **2** feature coordinatively unsaturated M^0 centers, we sought to explore the possibility of occupying the vacant coordination site with an additional equivalent

dx.doi.org/10.1021/ic2005248 |*Inorg. Chem.* 2011, 50, 5223–5233

Scheme 2

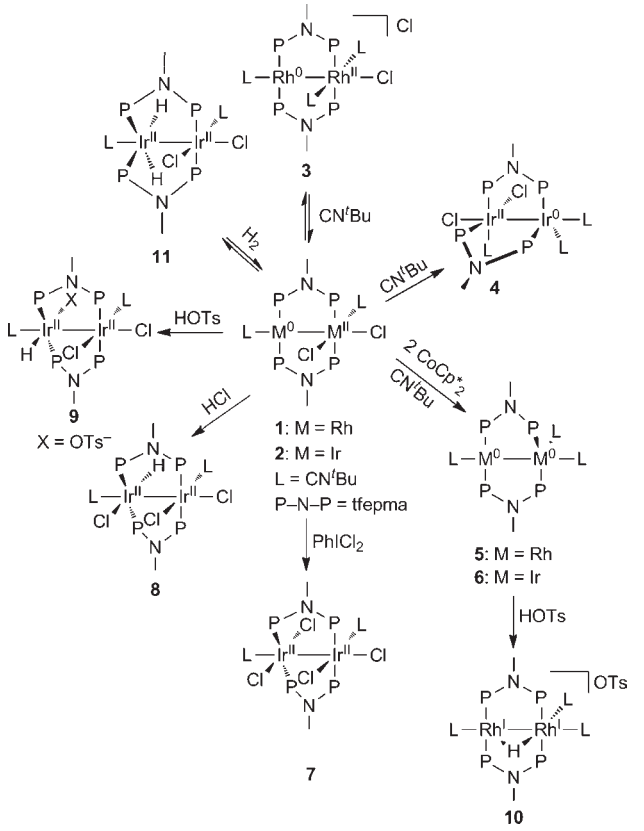

of CN^{t}Bu. Treatment of $Rh_2^{0,II}$ complex **1** with 1 equiv of CN^{t}Bu leads to reversible association of the added ligand, as judged by NMR spectra. The $^{31}P\{^1H\}$ spectrum, shown in Supporting Information, Figure S2, features broad resonances whose chemical shifts are nearly identical to parent complex **1**. The ^1H spectrum is similarly broadened and only shows a single *tert*-butyl resonance, offering little insight to the structure. UV−vis spectra of the isolated product, recorded in the range of 3−50 μM, are identical to that of complex **2**, suggesting complete dissociation of the additional CN^{t}Bu ligand at these low concentrations. X-ray crystallography reveals the structure of the addition product to be $[Rh_2^{0,II}(tfepma)_2(CN^tBu)_3Cl]Cl$ (**3**), shown in Figure 2. The incoming CN^{t}Bu ligand substitutes for one of the chloride ligands at the octahedral Rh^{II} center whereas the Rh^0 center is unperturbed. The intermetallic distances, 2.6847(10) Å and 2.6857(10) Å for the two crystallographically independent molecules, verify that the metal−metal bond and two-electron mixed valency are preserved upon ligand addition.

Treatment of $Ir_2^{0,II}$ complex **2** with 1 equiv of CN^{t}Bu in THF (Scheme 2) leads to a distinct outcome as compared to the addition chemistry of $Rh_2^{0,II}$ complex **1** with CN^{t}Bu. After 21 h, the $^{31}P\{^1H\}$ NMR spectrum of the crude reaction mixture shows a major product with three resonances—a multiplet at 102.6 ppm integrating to two phosphorus nuclei, and multiplets at 80.6 and 69.6 ppm each integrating to one phosphorus. These upfield resonances are attributed to the phosphorus nuclei coordinated to Ir^{II}, and their inequivalency suggests a cis arrangement of the phosphorus ligands at Ir^{II}. The solid state structure of $Ir_2^{0,II}(tfepma)_2(CN^tBu)_3Cl_2$ (**4**), shown in Figure 2, is consistent with this expectation. The Ir^0

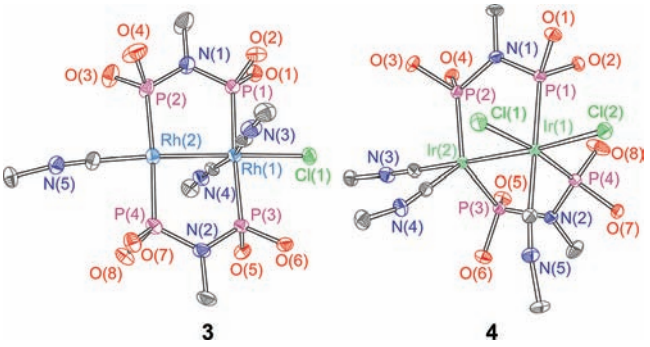

Figure 2. Thermal ellipsoid plots for **3** and **4**. Ellipsoids are shown at the 50% probability level with $-CH_2CF_3$ groups, CN^{t}Bu methyl groups, outer-sphere anions, and hydrogen atoms omitted for clarity. Data were collected at 100 ± 2 K.

center is now five-coordinate, distorted trigonal bipyramidal, and at the octahedral Ir^{II} center the two phosphorus atoms are cis to one another. The metal−metal distance has lengthened by 0.08 Å to 2.7920(3) Å, though this distance suggests that the metal−metal bond is intact.

When crystals of **4** are redissolved in acetonitrile, the NMR and UV−vis spectra suggest isomerization to a considerably more symmetric structure. The $^{31}P\{^1H\}$ NMR spectrum (Supporting Information, Figure S3) shows only two resonances, with an AA′XX′ splitting pattern. The spectrum is similar to that of parent $Ir_2^{0,II}$ complex **2** (Supporting Information, Figure S1), though the upfield resonance shifts by about 6 ppm and the multiplicity is distinct. The ^1H NMR spectrum features two closely spaced, sharp *tert*-butyl resonances with a 2:1 integration ratio, suggesting that all three CN^{t}Bu ligands remain bound. Furthermore, the UV−vis spectra of **2** (Supporting Information, Figure S13) and **4** (Supporting Information, Figure S14) are decidedly similar, with only slight 5−15 nm hypsochromic shifts of most peaks in the spectrum of **4** relative to that of **2**. These spectral data suggest that in acetonitrile solution, chloride dissociation from **4** leads to the ionic complex $[Ir_2^{0,II}(tfepma)_2(CN^tBu)_3Cl]Cl$, whose structure is analogous to **3**. The octahedral Ir^{II} and square planar Ir^0 sites possess similar coordination environments to the parent $Ir_2^{0,II}$ complex **2**, giving rise to only slightly differing spectral features.

Chemical Reduction of 1 and 2. Whereas treatment of $M_2^{0,II}$ complexes **1** and **2** with bis(cyclopentadienyl)cobalt(II) ($CoCp_2$, $E^{o\prime} = -1.33$ V) leads to incomplete reactions and mixtures of products, treatment with the stronger reducing agent bis(pentamethylcyclopenta-dienyl)cobalt(II) ($CoCp_2^*$, $E^{o\prime} = -1.94$ V)[23] completely consumes the $M_2^{0,II}$ starting material. Integration of the crude ^1H NMR spectra showed the major product of each reaction to contain three bound CN^{t}Bu ligands, and indeed optimized yields and purities of these major products, $M_2^{0,0}(tfepma)_2(CN^tBu)_3$ [M = Rh (**5**), Ir (**6**)], are obtained when complexes **1** and **2** are treated with both 2 equiv of $CoCp^*_2$ and 1 equiv of CN^{t}Bu, as described in Scheme 2. The solid state structures of compounds **5** and **6** are shown in Figure 3. An asymmetric structure is observed, with a four-coordinate, square planar environment about one M^0 center, and a five-coordinate, trigonal bipyramidal structure about the other. Metal−metal distances of 2.7099(5) Å (**5**) and 2.7631(4) Å (**6**) are observed for these formally d^9−d^9 complexes.

The room temperature NMR spectra of **5** and **6** suggest conformational fluxionality in solution. Although the solid state structure of both complexes would predict an asymmetric $^{31}P\{^1H\}$

dx.doi.org/10.1021/ic2005248 |*Inorg. Chem.* 2011, 50, 5223–5233

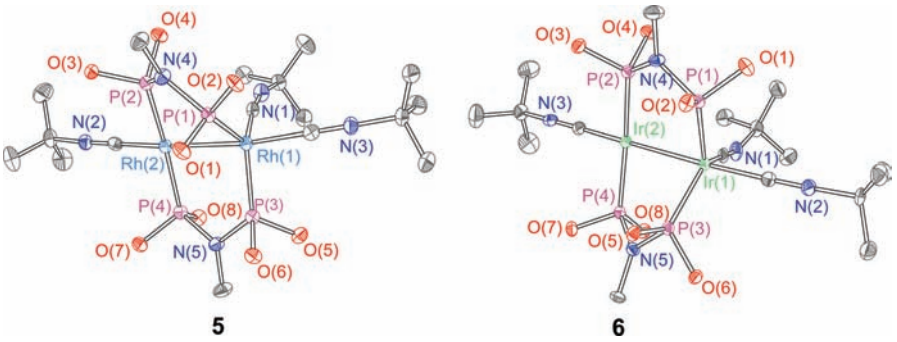

Figure 3. Thermal ellipsoid plots for **5** and **6**. Ellipsoids are shown at the 50% probability level with $-CH_2CF_3$ groups and hydrogen atoms omitted for clarity. Data were collected at 100 ± 2 K.

NMR spectrum, it (Supporting Information, Figures S4 and S5) shows a single resonance, which appears as a symmetric multiplet in **5** and a sharp singlet in **6**; the splitting in **5** arises from J_{P-Rh} coupling. In addition, the room temperature ^{1}H NMR spectra of **5** and **6** show a single *tert*-butyl resonance integrating to 27 protons, indicating that all three CN^{t}Bu ligands remain bound in solution, albeit in a fluxional manner. Variable temperature ^{1}H NMR, depicted in Figure 4 for the *tert*-butyl region of complex **6**, shows the evolution of two distinct *tert*-butyl resonances at low temperature, with a 2:1 (upfield:downfield) integration ratio. This behavior indicates that the four- and five-coordinate Ir^0 sites exchange slowly at low temperature, though even as low as −80 °C the two CN^{t}Bu ligands at the five-coordinate site rapidly exchange. The variable temperature ^{1}H NMR behavior for **5** (Supporting Information, Figure S22) is qualitatively the same, and for both complexes the remaining ^{1}H resonances are minimally perturbed as the temperature is altered. Variable temperature ^{31}P{^{1}H} NMR spectra, shown in Supporting Information, Figures S23 and S24, demonstrate considerable broadening as the temperature is lowered, but a single resonance is observed over the entire temperature range.

Chlorine Oxidation of 2. We have previously reported the synthesis and structure of $Rh_2^{II,II}(tfepma)_2(CN^tBu)_2Cl_4$, prepared by treatment of **1** with $PhICl_2$ in toluene.[20] In both solution and solid state, this $Rh_2^{II,II}$ complex (excluding $-OCH_2CF_3$ groups) adopts a centrosymmetric structure where both Rh^{II} sites are equivalent. In contrast, treatment of diiridium complex **2** with $PhICl_2$ leads to nearly exclusive formation of an asymmetric oxidation product. The ^{31}P{^{1}H} NMR spectrum of $Ir_2^{II,II}(tfepma)_2(CN^tBu)_2Cl_4$ (**7**), shown in Supporting Information, Figure S6, reveals two closely spaced multiplets, which are related by a mirror plane and suggestive of an AA′BB′ spin system for which 12 of the possible 24 lines[24] are resolved. A very minor product (<5%), present in both the crude reaction mixture and the isolated material, appears as a singlet in the ^{31}P{^{1}H} spectrum, consistent with a small amount of the centrosymmetric isomer being formed. The ^{1}H NMR spectrum also reveals asymmetry—two distinct *tert*-butyl peaks, each integrating to nine protons, are evident.

The solid state X-ray structure of **7** presented in Figure 5 confirms the asymmetric structure predicted by NMR. Two nearly octahedral Ir^{II} centers separated by an intermetallic distance of 2.7774(3) Å are observed. The chloride ligands about Ir(1) maintain the cis arrangement found in $Ir_2^{0,II}$ complex **2** (see Figure 1), whereas on Ir(2) the chloride ligands are trans to one another, with an axial CN^{t}Bu ligand. The complex clearly lacks the inversion center found in the analogous $Rh_2^{II,II}$ version, giving rise to the asymmetry observed in the NMR spectra.

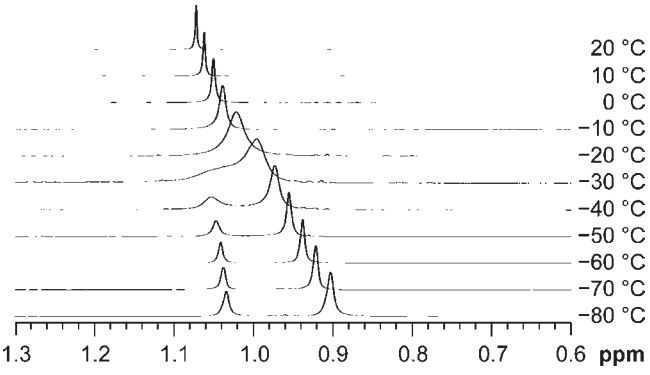

Figure 4. Variable temperature ^{1}H NMR spectra for complex **6**, showing the *tert*-butyl resonances. Spectra were recorded in toluene-d_8 at 500 MHz.

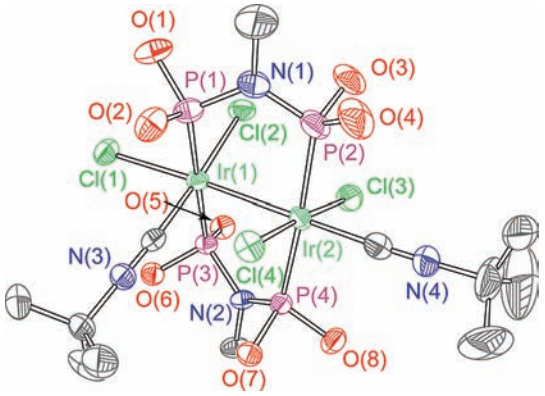

Figure 5. Thermal ellipsoid plot for **7**. Ellipsoids are shown at the 50% probability level with $-CH_2CF_3$ groups and hydrogen atoms omitted for clarity. Data were collected at 183 ± 2 K.

Protonation of 2 with HX (X = Cl$^-$, OTs$^-$). Reversible protonation of dirhodium complex **1** with HCl has been detailed previously,[20] and we reasoned that analogous complexes could be accessed from $Ir_2^{0,II}$ complex **2**. By treating **2** with either HCl or lutidinium hydrochloride (LutH$^+$Cl$^-$), a single isomer of $Ir_2^{II,II}(tfepma)_2(CN^tBu)_2Cl_3H$ (**8**) is formed rapidly and quantitatively. The ^{31}P{^{1}H} NMR spectrum (Supporting Information, Figure S7) again shows two multiplets attributed to an AA′BB′ spin system; in this case 20 of the 24 possible lines are resolved. The most definitive evidence for the presence of an iridium-bound

dx.doi.org/10.1021/ic2005248 |*Inorg. Chem.* 2011, 50, 5223–5233

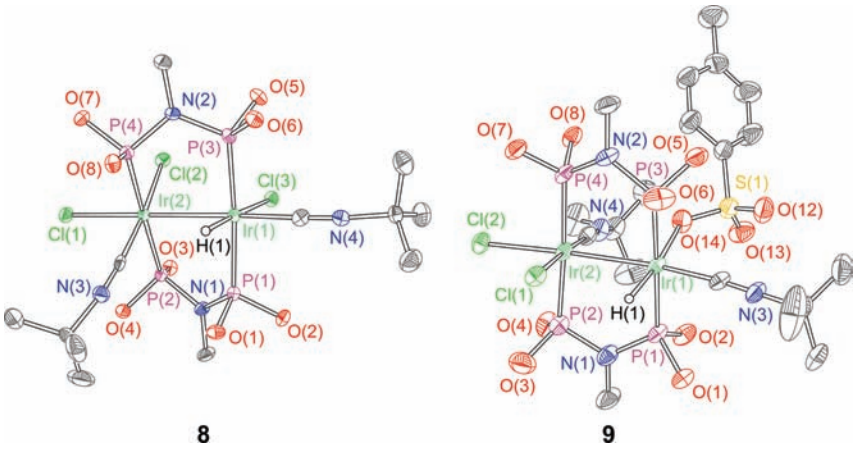

Figure 6. Thermal ellipsoid plots for **8** and **9**. Ellipsoids are shown at the 50% (**8**) or 30% (**9**) probability level with $-CH_2CF_3$ groups, solvent atoms and carbon-bound hydrogen atoms omitted for clarity. Data was collected at 100 ± 2 K (**8**) and 175 ± 2 K (**9**).

hydride comes from the ^{1}H NMR, which shows a 1:2:1 triplet at −20.69 ppm. This hydride peak integrates to one proton, and the observed $^2J_{H-P}$ of 16.0 Hz indicates that the hydride is positioned cis to two equivalent phosphorus atoms. The solid state structure of **8**, shown in Figure 6, is analogous to that of **7**, with a hydride replacing one of the chlorides. Both Ir^{II} centers are again octahedral, and hydride ligand H(1) is arranged trans to Cl(3) and syn with respect to the CN^{t}Bu ligand on the adjacent Ir^{II} center. The metal−metal distance is 2.7821(3) Å, and the strong trans influence of the hydride ligand is readily apparent. The Ir(1)−Cl(3) bond, situated trans to the hydride, has a distance of 2.5021(11) Å, which is substantially longer than the other equatorial chloride bond distance [Ir(2)−Cl(2)] (d = 2.4002(10) Å).

Addition of HOTs to **2** proceeds readily, and when carried out in acetonitrile, the ^{1}H NMR reveals two hydride-containing products in about a 1:1 ratio. By changing the reaction solvent to THF, a 9:1 ratio of the two products is obtained for the isolated product. The major isomer of $Ir_2^{II,II}(tfepma)_2(CN^tBu)_2Cl_2H(OTs)$ can be crystallized. Its structure, which is shown in Figure 6, bears many similarities to its HCl-addition analogue, namely, an axial CN^{t}Bu ligand and a trans arrangement of the H(1) and OTs^- ligands at the site of protonation. The major difference between the structures of **8** and **9** is the position of the hydride relative to the CN^{t}Bu ligand on the adjacent iridium; for **9**, the hydride is in an anti conformation relative to the vicinal CN^{t}Bu. Additionally, the metal−metal distance in **9** at 2.7573(5) Å is slightly contracted relative to **8**. The ^{31}P NMR spectrum of tosylate complex **9** (Supporting Information, Figure S8) is again characteristic of an AA′BB′ spin system, and its ^{1}H NMR spectrum shows an Ir−H resonance at −20.00 ppm, only marginally upfield relative to the hydride resonance of **8**. The observed $^2J_{H-P}$ coupling constant in **9** is identical to that of **8** at 16.0 Hz. As alluded to above, when **9** is isolated about 10% of a minor isomer is present. The minor product shows a hydride resonance at −20.71 ppm in the ^{1}H spectrum, and yet again the two-bond proton-phosphorus coupling constant is 16.0 Hz, placing the hydride cis to its neighboring phosphorus nuclei. The remaining ^{31}P and ^{1}H NMR features of the minor isomer are virtually identical to those of the major product, suggesting an identical structure but with the hydride flipped to the other side of the metal−metal axis to position it syn to the vicinal CN^{t}Bu. This isomerization will produce the same structure as that of

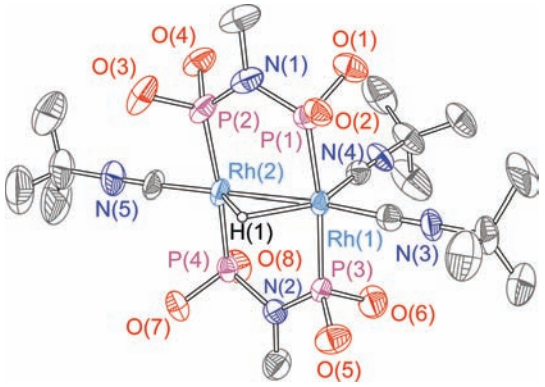

Figure 7. Thermal ellipsoid plot for the cation of **10**. Ellipsoids are shown at the 50% probability level with $-CH_2CF_3$ groups, the outer-sphere tosylate anion and carbon-bound hydrogen atoms omitted for clarity. Data were collected at 100 ± 2 K.

hydrido-chloride complex **8**, but with the chloride trans to the hydride substituted for OTs^-. We cannot rule out other possibilities such as intermetallic exchange of Cl^- and OTs^-, though the simple isomerization described above seems most plausible for the structure of the minor product.

Protonation of 5 with HOTs. Reactions involving $M_2^{0,0}$ complexes **5** and **6** were explored with a variety of acids, though in most cases, complex and intractable mixtures of products were formed. The lone exception was the exclusive production of $[Rh_2^{I,I}(tfepma)_2(CN^tBu)_3(\mu\text{-}H)](OTs)$ (**10**), obtained from the treatment of $Rh_2^{0,0}$ complex **5** with 1 equiv of HOTs in thawing acetonitrile. The crystal structure of **10** is depicted in Figure 7. The position of the hydride ligand could not be located precisely, and the refinement statistics were indistinguishable if the hydride was modeled either as bridging or as a terminal hydride on Rh(1). However, on the basis of the NMR data (vide infra), complex **10** is assigned as a $Rh^I\cdots Rh^I$ μ-hydride species, as shown in Figure 7. All three CN^{t}Bu ligands remain bound, and the intermetallic distance of 2.7449(11) Å compares favorably with other hydride-bridged dirhodium complexes spanned by two diphosphines.[25−27] The OTs^- counterion is outer-sphere and does not interact with the cationic complex in the crystal structure.

Both the $^{31}P\{^1H\}$ and the ^{1}H NMR spectra support the assignment of a valence symmetric structure for **10**. The ^{31}P

dx.doi.org/10.1021/ic2005248 |*Inorg. Chem.* 2011, 50, 5223–5233

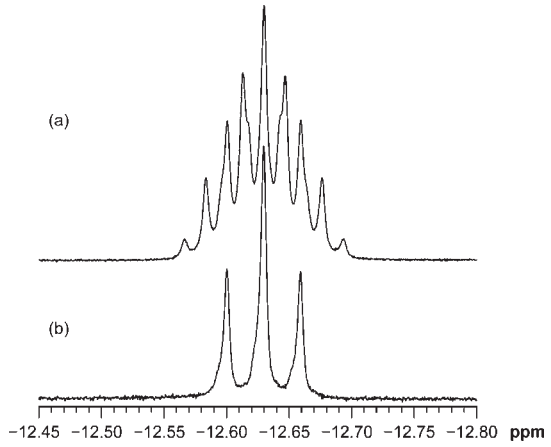

Figure 8. ^{1}H (a) and $^{1}H\{^{31}P\}$ (b) NMR spectra of **10**, showing the Rh−*H* resonance. Spectra were recorded in CD_3CN at 500 MHz and 293 K.

NMR spectrum (Supporting Information, Figure S9) shows a single, symmetric multiplet centered at 150.7 ppm with a splitting pattern reminiscent of $Rh_2^{0,0}$ precursor **6**. This contrasts the expected four-spin, second-order system expected for a two-electron mixed-valence state (vide supra). In the room temperature ^{1}H NMR spectrum, a single, sharp *tert*-butyl resonance is observed, which splits into two distinct peaks at low temperature, as shown in Supporting Information, Figure S25. The most definitive evidence for a bridging hydride ligand comes from the low-frequency region of the ^{1}H NMR spectrum. As shown Figure 8a, in the ^{1}H NMR spectrum the rhodium-hydride resonance appears as a complex, symmetric multiplet, with 9 lines clearly resolved and an additional 4 lines appearing as shoulders. In the $^{1}H\{^{31}P\}$ spectrum (Figure 8b), only coupling to ^{103}Rh is observed, and a triplet splitting pattern results. This triplet multiplicity indicates equal coupling to both rhodium nuclei, with a $^{1}J_{H-Rh}$ of 14.8 Hz, and accordingly places the hydride in a bridging position. The remainder of the multiplet in the phosphorus-coupled ^{1}H spectrum is generated by considering equal coupling of the hydride nucleus to all four phosphorus nuclei, with an observed $^{2}J_{H-P}$ of 8.5 Hz. This value is considerably smaller than the $^{2}J_{H-P}$ coupling constants in bimetallic complexes of similar architectures featuring terminal hydride complexes.[11,20] This arrangement of coupling constants would give a maximum of 15 lines in a triplet of quintets pattern, 13 of which are resolved in the phosphorus-coupled spectrum.

Reaction of 2 with H_2. When a solution of **2** in THF-d_8 is introduced to about 1.5 atm of H_2, the bright orange color rapidly fades to give a nearly colorless solution. NMR spectroscopy shows clean conversion to $Ir_2^{II,II}(tfepma)_2(CN^tBu)_2Cl_2(H)_2$ (**11**). The $^{31}P\{^{1}H\}$ NMR spectrum (Supporting Information, Figure S10) and the N−C*H*$_3$ and *tert*-butyl regions of the ^{1}H spectrum (Supporting Information, Figure S11) clearly show two isomers, formed in about a 19:1 ratio. The low-frequency region of the ^{1}H NMR spectrum, reproduced in Figure 9, gives some insight into the structural differences between the two isomers. The major product shows a complex, asymmetric multiplet integrating to two protons centered at about −12.3 ppm. The large 187 Hz splitting between the two most intense peaks suggests the presence of trans $^{2}J_{H-P}$ coupling. Though the precise structure of the major product was not elucidated from NMR spectra, it has been structurally characterized by X-ray crystallography as detailed below.

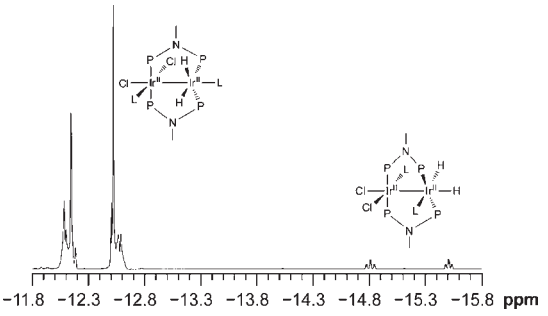

Figure 9. Low-frequency region of the ^{1}H NMR spectrum of **11**, showing the Ir−*H* resonances for the major and minor isomers. The structure of the major isomer and a likely structure of the minor isomer are shown near the peaks they are assigned to.

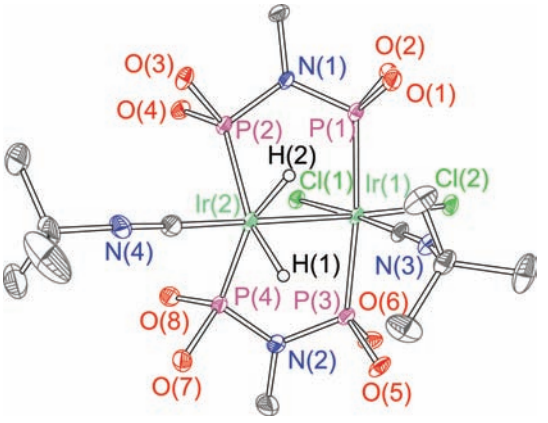

Figure 10. Thermal ellipsoid plot of **11**. Ellipsoids are shown at the 50% probability level with $-CH_2CF_3$ groups and carbon-bound hydrogen atoms omitted for clarity. Data were collected at 100 ± 2 K.

For the minor product, the two hydride ligands are chemically inequivalent, with a straightforward triplet of doublets splitting pattern for each resonance. The two peaks have slightly different $^{2}J_{H-P}$ coupling constants: the downfield resonance (−14.80 ppm) has a value of 17.9 Hz whereas the upfield resonance (−15.50 ppm) is coupled to phosphorus with a 13.8 Hz coupling constant. These two values indicate that each of the inequivalent hydrides is arranged cis to the two adjacent phosphorus nuclei. The doublet splitting results from $^{2}J_{H-H}$ coupling of the two hydride ligands, and a coupling constant of 4.6 Hz indicates a cis arrangement of the two hydrides as observed for numerous other cis dihydride complexes of iridium.[28−32] One of the two resonances for this minor isomer is clearly visible in the $^{31}P\{^{1}H\}$ NMR spectrum (Supporting Information, Figure S10), and its appearance as an AA′XX′ multiplet suggests a trans arrangement of the two phosphorus nuclei at each iridium. A likely structure for this minor product is included in Figure 9, though a structure in which the equatorial hydride is switched with the CN^tBu (L) trans to it would also be consistent with the spectral data. Solutions of **11** are unstable with respect to H_2 loss. The orange color and NMR features of $Ir_2^{0,II}$ complex **2** are restored by repeated freeze−pump−thaw cycling of a solution of **11** or by removing all volatiles and drying in vacuo.

The major isomer of **11** was crystallized from CD_3CN under an H_2 atmosphere, and its structure has been determined unequivocally by single crystal X-ray diffraction, as shown in

dx.doi.org/10.1021/ic2005248 |*Inorg. Chem.* 2011, 50, 5223–5233

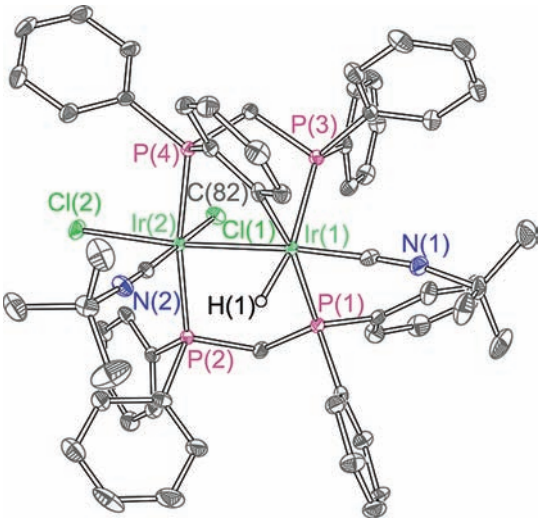

Figure 11. Thermal ellipsoid plot of **12**. Ellipsoids are shown at the 50% probability level with the solvent molecule and carbon-bound hydrogen atoms omitted for clarity. Data were collected at 100 ± 2 K.

Figure 10. Both iridium centers are six-coordinate, with a cis-P_2, cis-H_2 geometry at Ir(1). The geometry about Ir(1) is substantially distorted from octahedral, marked by a P(2)−Ir(2)−P(4) angle of 118.46(5)° and a H(1)−Ir(2)−H(2) angle of 79(3)°. The H(1)−H(2) distance is 2.04(7) Å, with an Ir(1)−Ir(2) bond distance of 2.7487(3) Å similar to the other metal−metal bonded $Ir_2^{II,II}$ complexes described herein.

Bimetallic Iridium Hydride Complex Formation by Cyclometalation. In the course of preparing $M_2^{0,II}$ complexes **1** and **2**, we sought similar complexes bearing other bridging phosphine ligands. Reaction of $[Ir^I(COD)Cl]_2$ with 2 equiv of dppm and 2 equiv of CN^tBu in THF leads to immediate formation of a dark green solution, followed by the gradual deposition of a cream-colored solid, identified spectroscopically and crystallographically as $Ir_2^{II,II}(dppm)(PPh(o\text{-}C_6H_4)CH_2PPh_2)(CN^tBu)_2Cl_2H$ (**12**), which bears the expected stoichiometry but involves an intermetallic cyclometalation of one dppm ligand. The solid state structure is depicted in Figure 11. The most noteworthy feature is the orthometalation of a phenyl ring bonded to P(4) onto the opposite iridium site, Ir(1). The phenyl and hydride ligands are arranged cis to one another, and again the geometry is distorted from octahedral. The P(1)−Ir(1)−P(3) angle is 109.83(3)° whereas the C(82)−Ir(1)−H(1) angle is 81.4(13)°, giving a coordination geometry similar to that of **11**. The Ir(1)−Ir(2) distance is 2.7928(4) Å.

Complex **12** suffers from limited solution stability, decomposing to an intractable mixture of products within hours. However, the NMR spectra of **12** do suggest that prior to decomposition, the solid-state structure is maintained in solution, and that the C−H activation is irreversible at room temperature. The $^{31}P\{^1H\}$ NMR spectrum (Supporting Information, Figure S12) shows three distinct chemical environments for the phosphorus nuclei, with complex multiplicity in all of the peaks. In addition to the expected ^1H NMR resonances arising from dppm and CN^tBu protons, a doublet of doublets integrating to one proton is seen at −10.69 ppm for the iridium-hydride. The $^2J_{H-P}$ values of 163 and 19.1 Hz are indicative of coupling of the hydride nucleus to a trans and cis phosphorus nucleus, respectively. Furthermore, the dppm $-CH_2-$ resonances are each split into two distinct frequencies, suggestive of the very rigid binding mode of the bridging ligands.

UV−vis Absorption Spectra. Excepting complexes **3** and **12**, which are unstable in dilute solution, the UV−vis absorption features of all new compounds are collected in Supporting Information, Figures S13−S21. The electronic spectrum of $Ir_2^{0,II}$ complex **2** (Supporting Information, Figure S13) is decidedly more complex than that of dirhodium analogue **1**,[20] with 6 closely spaced, overlapping but resolved bands. This complexity is mirrored in $Ir_2^{0,II}$ complex **3** (Supporting Information, Figure S14), which is prepared by CN^tBu addition to **2** and presumed to have a similar solution structure in acetonitrile, giving rise to similar absorption features as discussed above. The absorption spectra of $M_2^{0,0}$ complexes **5** and **6** (Supporting Information, Figure S15 and S16) also share similarities with one another, showing a maximum at 379 nm in dirhodium complex **5** and 383 nm in diiridium complex **6**, along with a shoulder toward the visible region and intense UV features. Complexes **7**−**9** and **11** all feature a d^7-d^7 $Ir_2^{II,II}$ core and have largely analogous absorption profiles. All show two distinct maxima and a shoulder (Supporting Information, Figures S17−S19, S21) whose positions are marginally responsive to the ligand environment. In all cases the highest energy peak is the wavelength of maximum absorption, which ranges between 267 nm (**11**) and 285 nm (**8**). The electronic spectrum of dirhodium μ-hydride **10**, shown in Supporting Information, Figure S20, shows a series of five closely spaced overlapping absorption bands. In addition to the electronic absorption features described above, the $Ir_2^{0,II}$ and $Ir_2^{II,II}$ complexes **2**, **3**, and **7**−**9** are emissive at 77 K in 2-methyltetrahydrofuran solution. The emission bands are about 600 nm, with maxima at 613 nm (**2**), 598 nm (**3**), 624 nm (**7**), 641 nm (**8**), and 582 nm (**9**). For the $Ir_2^{II,II}$ complexes **7**−**9**, the relative energies of the emission maxima track well with the energy of the absorption maxima, and in all cases the large Stokes shifts suggest emission from a triplet excited state.

DISCUSSION

Two-electron mixed valence dirhodium and diiridium complexes can serve as platforms for a diverse range of chemistries, including photocatalytic H_2 production,[3,4] multielectron photochemistry,[5,6] reversible H_2 addition,[33] C−H activation,[34] and other organometallic chemistry.[35] In all of these previous examples, the $M_2^{0,II}$ complexes contain M^0 centers that are five-coordinate, precluding reactivity at this reduced metal site. We reasoned that addition reactions could be facilitated by preparing two-electron mixed valence group 9 bimetallic complexes with four-coordinate M^0 sites. Complexes **1** and **2**, which meet this criterion, assemble readily when $[M^I(COD)Cl]_2$ (M = Rh, Ir) is treated with 2 equiv of tfepma and 2 equiv of CN^tBu. The net result is valence disproportionation of the $M_2^{I,I}$ precursor to yield $M_2^{0,II}(tfepma)_2(CN^tBu)_2Cl_2$ [M = Rh (**1**), Ir (**2**)]. The coordinative unsaturation at the M^0 site in **1** and **2** drives the binding of donor ligands such as CN^tBu to furnish complex **4**. In the solid state, **4** contains three bound CN^tBu molecules, indicating that the open coordination site at the Ir^0 center in **2** can accept an additional ligand. However, the solution behavior of **4**, and the disparate reactivity of $Rh_2^{0,II}$ complex **1** toward CN^tBu revealed some unexpected results concerning ligand addition and substitution. When **1** is treated with CN^tBu, the broadened NMR features suggest reversible binding to form **3**. Crystals of **3** revealed the unexpected structure shown in Figure 2, where the reaction results in ligand substitution instead of addition.

dx.doi.org/10.1021/ic2005248 |*Inorg. Chem.* 2011, 50, 5223–5233

The equatorial Cl^- ligand at the Rh^{II} site is displaced by the incoming CN^tBu, maintaining the square planar Rh^0 and octahedral Rh^{II} geometries that are found in **1**. This suggests that the electrophilicity of the Rh^{II} center dictates the reactivity, as opposed to the vacant coordination site at Rh^0. The NMR and UV−vis spectra of diiridium complex **4** indicate that a structure analogous to dirhodium analogue **3** results when **4** is dissolved in acetonitrile. These results reveal that in the two-electron mixed valence state a four-coordinate M^0 center is quite favorable, even when the possibility of forming a five-coordinate center exists.

We have demonstrated that multielectron photocatalytic processes are enabled when the bimetallic catalyst can span multiple oxidation states differing by two electrons each.[3,4] Thus, the ability to prepare a homologous series of d^7-d^7, d^7-d^9, and d^9-d^9 complexes motivate future studies of multielectron catalysis supported on the complexes described here. Indeed, $M_2^{0,II}$ complexes **1** and **2** may be both reduced and oxidized by two electrons to prepare the full suite of oxidation states. Our initial goal was to reduce **1** and **2** to complexes of the stoichiometry $M_2^{0,0}(tfepma)_2(CN^tBu)_2$, which would feature two four-coordinate M^0 sites. However, such species are not observed, and isostructural complexes $M_2^{0,0}(tfepma)_2(CN^tBu)_3$ [M = Rh (**5**), Ir (**6**)], are instead obtained where an additional equivalent of CN^tBu is required to stabilize the fully reduced core. Nevertheless, the structures of **5** and **6** (Figure 3) each reveal a four-coordinate M^0 center, motivating further study of demanding addition reactions on these highly reducing species. Oxidation of **2** with $PhICl_2$ produces $Ir_2^{II,II}(tfepma)_2(CN^tBu)_2Cl_4$ (**7**), which is structurally distinct from its dirhodium analogue.[20]

Having established a redox chemistry of **1** and **2**, routes for the preparation of hydride-containing complexes are available. Protonation reactions of isoelectronic valence-symmetric dirhodium A-frame complexes have been shown to give products featuring a bridging hydride, where the net reaction is the protonation of the metal−metal bond.[26] The reactivity of our first-generation $Ir_2^{0,II}$ complexes[33] arises from a vacant axial site on the M^{II} center. Reagents such as HX and H_2 result in oxidative addition across the metal−metal bond, with two-electron mixed valency preserved in the products. In contrast, addition of HX ($X = Cl^-$, OTs^-) and H_2 to **2** furnishes products suggestive of addition to the Ir^0 site, and the Ir^{II} center unperturbed. As seen in the crystal structures of $Ir_2^{II,II}(tfepma)_2(CN^tBu)_2Cl_2HX$ [$X = Cl^-$ (**8**), OTs^- (**9**)], the hydride and X^- ligand situate in a trans configuration on the same metal center, and a valence-symmetric $Ir_2^{II,II}$ core ensues. Only terminal hydride products are observed for these acid addition reactions. $Ir_2^{0,II}$ complex **2** reacts much more readily with HX than its dirhodium analogue **1**. HCl addition to **1** is decidedly reversible[20] whereas in the case of **2** a single equivalent of HCl begets quantitative formation of hydride-containing **8**. In addition, $Ir_2^{II,II}Cl_3H$ complex **8** is conveniently prepared by protonation of **2** with solid HCl surrogate $LutH^+Cl^-$, though dirhodium complex **1** is completely unreactive to this reagent. This difference in reactivity is likely tied to the stronger iridium-hydride bond strengths as compared to rhodium.[36] Attempted protonation reactions of $M_2^{0,0}$ complexes **5** and **6** were generally not fruitful, though $Rh_2^{0,0}$ complex **5** does react readily with HOTs to furnish μ-hydride complex **10** (Figure 7). This outcome is largely reminiscent of earlier examples of protonation reactions involving other group 9 $M_2^{0,0}$ complexes, where the addition of acid also gives a hydride-bridged product and an outer-sphere conjugate base anion.[25,37,38]

The hydrogenation reaction of **2** is also distinct from that of previous diiridium constructs. Several products have been identified from hydrogenation reactions of valence-symmetric diiridium

Scheme 3

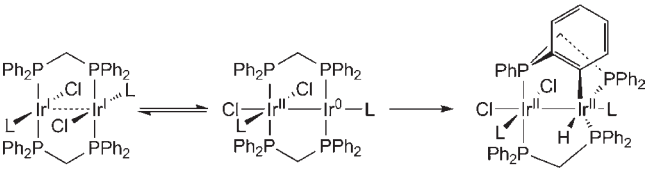

complexes. Hydrogenation of a face-to-face diiridium(I) complex yields a vicinal dihydride product, where the two terminal hydride ligands are syn with respect to each other.[39] When diiridium A-frame complexes are treated with H_2 the thermodynamically stable species is once again a vicinal dihydride, though in this case the two H^- ligands occupy axial positions;[39,40] it has since been shown that a geminal cis-dihydride forms initially which rearranges to this final product.[41,42] In our earlier work on two-electron mixed-valence complexes,[33] hydrogenation of the iridium−iridium bond was observed, producing a vicinal dihydride where the two electron mixed valency was preserved in a formally $Ir^I \rightarrow Ir^{III}$ core. The addition of H_2 to **2**, where the coordinative unsaturation resides at the four-coordinate Ir^0 center, produces a result distinct from these previously characterized reactions. In the same vein as the HX addition reactions, H_2 adds to a single metal center, resulting in an $Ir_2^{II,II}$ geminal cis-dihydride product **11**, whose structure is depicted in Figure 10, as well as a minor product which also features a cis-dihydride arrangement. On the basis of X-ray crystallography and ^1H NMR spectroscopy we see no evidence for rearrangement to vicinal dihydride isomers. The distance between the two hydrogen nuclei (d = 2.04(7) Å) indicates that the H−H bond is cleaved completely and that the description of **11** as a dihydride complex is valid.[43] The cis arrangement of the hydride ligands in **11**, compared to the trans HX complexes described above, suggests the possibility of a different mechanism for H_2 and HX oxidative additions. H_2 addition is clearly reversible, and removal of the H_2 headspace from a solution of **11** regenerates complex **2** cleanly.

A route to a diiridium hydride complex is also achieved from intramolecular cyclometalation. With the bridging ligand dppm and reaction conditions otherwise identical to the synthesis of **2**, the complex $Ir_2^{II,II}(dppm)(PPh(o\text{-}C_6H_4)CH_2PPh_2)(CN^tBu)_2Cl_2H$ (**12**) is formed as the final product. At early reaction time a dark green solution is observed, which is qualitatively indicative of an initial $Ir^I\cdots Ir^I$ product prior to the cyclometalation. The final product possesses an $Ir^{II,II}$ core oxidation state with the expected stoichiometry (Figure 11). The cyclometalated binding mode of dppm seen in the structure of **12** has been observed in a Cp*-ligated diiridium complex,[44] where an ortho C−H bond was activated in a base-assisted fashion. Although the mechanism of cyclometalation of **11** has not been probed in detail, a plausible route is shown in Scheme 3. The initially formed $Ir^I\cdots Ir^I$ complex rearranges to an $Ir_2^{0,II}$ state, and cyclometalation at the reactive Ir^0 center yields **11**. Direct cyclometalation of $Ir^I\cdots Ir^I$ cannot be explicitly ruled out, though a more complex mechanism involving chloride-bridged intermediates and/or phosphine dissociation would be required to avoid hypercoordinate intermediate species.

To summarize, we have demonstrated a multifaceted reaction chemistry centered around coordinatively unsaturated two-electron mixed valence dirhodium and diiridium complexes. We have shown that stable complexes with d^9-d^9, d^7-d^9, and d^7-d^7 electron counts can all be prepared with the ligand framework

dx.doi.org/10.1021/ic2005248 |Inorg. Chem. 2011, 50, 5223–5233

employed here. Three distinct routes to access hydride-containing products are outlined—addition of HX (X = Cl^-, OTs^-), addition of H_2, and intramolecular cyclometalation. On account of the coordinative unsaturation at Ir^0, both HX and H_2 oxidative addition furnish hydride-containing products with novel structures; these complexes are candidates for future HX splitting schemes. In addition, hydrido-halide complex **8** is a structural analogue to a dirhodium analogue which mediates O_2 reduction to water.[20] The O_2 reactivity of the diiridium hydride complexes shown here is under active investigation with the objective of providing insight into the mechanism of O_2 reduction. Our interest in bimetallic hydride-containing complexes is ongoing, as we continue to explore their reactivity and unveil new routes for their facile preparation.

■ ASSOCIATED CONTENT

Ⓢ Supporting Information. $^{31}P\{^1H\}$ NMR spectra for all complexes, partial ^1H NMR spectrum of **11**, electronic absorption and emission spectra for **2** and **4**—**11**, variable temperature NMR spectra of **5**, **6**, and **10**, X-ray crystallographic data table, and the crystallographic information file (CIF). This material is available free of charge via the Internet at http://pubs.acs.org.

■ AUTHOR INFORMATION

Corresponding Author
*E-mail: nocera@mit.edu.

■ ACKNOWLEDGMENT

This work was supported by NSF Grant CHE-0750239. Grants from the NSF also supported the MIT Department of Chemistry Instrumentation Facility (CHE-9808061 and DBI-9729592). T.S.T. acknowledges the Fannie and John Hertz Foundation for a graduate research fellowship.

■ REFERENCES

(1) Cook, T. R.; Dogutan, D. K.; Reece, S. Y.; Surendranath, Y.; Teets, T. S.; Nocera, D. G. *Chem. Rev.* **2010**, *110*, 6472–6502.
(2) Esswein, A. J.; Nocera, D. G. *Chem. Rev.* **2007**, *107*, 4022–4047.
(3) Heyduk, A. F.; Nocera, D. G. *Science* **2001**, *293*, 1639–1641.
(4) Esswein, A. J.; Veige, A. S.; Nocera, D. G. *J. Am. Chem. Soc.* **2005**, *127*, 16641–16651.
(5) Heyduk, A. F.; Macintosh, A. M.; Nocera, D. G. *J. Am. Chem. Soc.* **1999**, *121*, 5023–5032.
(6) Odom, A. L.; Heyduk, A. F.; Nocera, D. G. *Inorg. Chim. Acta* **2000**, *297*, 330–337.
(7) Cook, T. R.; Esswein, A. J.; Nocera, D. G. *J. Am. Chem. Soc.* **2007**, *129*, 10094–10095.
(8) Cook, T. R.; Surendranath, Y.; Nocera, D. G. *J. Am. Chem. Soc.* **2009**, *131*, 28–29.
(9) Teets, T. S.; Nocera, D. G. *J. Am. Chem. Soc.* **2009**, *131*, 7411–7420.
(10) Teets, T. S.; Lutterman, D. A.; Nocera, D. G. *Inorg. Chem.* **2010**, *49*, 3035–3043.
(11) Teets, T. S.; Neumann, M. P.; Nocera, D. G. *Chem. Commun.* **2011**, *47*, 1485–1487.
(12) Roseblade, S. J.; Pfaltz, A. *Acc. Chem. Res.* **2007**, *40*, 1402–1411.
(13) Heiden, Z. M.; Rauchfuss, T. B. *J. Am. Chem. Soc.* **2007**, *129*, 14303–14310.
(14) Wick, D. D.; Goldberg, K. I. *J. Am. Chem. Soc.* **1999**, *121*, 11900–11901.
(15) Denney, M. C.; Smythe, N. A.; Cetto, K. L.; Kemp, R. A.; Goldberg, K. I. *J. Am. Chem. Soc.* **2006**, *128*, 2508–2509.
(16) Konnick, M. M.; Gandhi, B. A.; Guzei, I. A.; Stahl, S. S. *Angew. Chem., Int. Ed.* **2006**, *45*, 2904–2907.
(17) Konnick, M. M.; Stahl, S. S. *J. Am. Chem. Soc.* **2008**, *130*, 5753–5762.
(18) Morris, A. J.; Meyer, G. J.; Fujita, E. *Acc. Chem. Res.* **2009**, *42*, 1983–1994.
(19) McGrady, G. S.; Guilera, G. *Chem. Soc. Rev.* **2003**, *32*, 383–392.
(20) Teets, T. S.; Cook, T. R.; McCarthy, B. D.; Nocera, D. G. *J. Am. Chem. Soc.*, DOI: 10.1021/ja201972v.
(21) Teets, T. S.; Cook, T. R.; Nocera, D. G. *Inorg. Synth.* **2010**, *35*, 164–168.
(22) Zielinska, A.; Skulski, L. *Tetrahedron Lett.* **2004**, *45*, 1087–1089.
(23) Connelly, N. G.; Geiger, W. E. *Chem. Rev.* **1996**, *96*, 877–910.
(24) Hesse, M.; Meier, H.; Zeeh, B. *Spectroscopic Methods in Organic Chemistry*, 2nd ed.; Thieme: Stuttgart, 2008; p 85.
(25) Kubiak, C. P.; Woodcock, C.; Eisenberg, R. *Inorg. Chem.* **1982**, *21*, 2119–2129.
(26) Sutherland, B. R.; Cowie, M. *Inorg. Chem.* **1984**, *23*, 1290–1297.
(27) Werner, H.; Manger, M.; Laubender, M.; Teichert, M.; Stalke, D. *J. Organomet. Chem.* **1998**, *569*, 189–194.
(28) Gründemann, S.; Kovacevic, A.; Albrecht, M.; Faller, J. W.; Crabtree, R. H. *J. Am. Chem. Soc.* **2002**, *124*, 10473–10481.
(29) Clot, E.; Chen, J.; Lee, D.-H.; Sung, S. Y.; Appelhans, L. N.; Faller, J. W.; Crabtree, R. H.; Eisenstein, O. *J. Am. Chem. Soc.* **2004**, *126*, 8795–8804.
(30) Clarke, Z. E.; Maragh, P. T.; Dasgupta, T. P.; Gusev, D. G.; Lough, A. J.; Abdur-Rashid, K. *Organometallics* **2006**, *25*, 4113–4117.
(31) Atkinson, K. D.; Cowley, M. J.; Duckett, S. B.; Elliott, P. I. P.; Green, G. R. G.; López-Serrano, J.; Khazal, I. G.; Whitwood, A. C. *Inorg. Chem.* **2009**, *48*, 663–670.
(32) Nishihara, Y.; Takemura, M.; Osakada, K. *Inorg. Chim. Acta* **2009**, *362*, 2951–2956.
(33) Heyduk, A. F.; Nocera, D. G. *J. Am. Chem. Soc.* **2000**, *122*, 9415–9426.
(34) Esswein, A. J.; Veige, A. S.; Piccoli, P. M. B.; Schultz, A. J.; Nocera, D. G. *Organometallics* **2008**, *27*, 1073–1083.
(35) Veige, A. S.; Gray, T. G.; Nocera, D. G. *Inorg. Chem.* **2005**, *44*, 17–26.
(36) Pearson, R. G. *Chem. Rev.* **1985**, *85*, 41–49.
(37) Sutherland, B. R.; Cowie, M. *Organometallics* **1985**, *4*, 1637–1648.
(38) Jenkins, J. A.; Cowie, M. *Organometallics* **1992**, *11*, 2767–2774.
(39) Sutherland, B. R.; Cowie, M. *Organometallics* **1985**, *4*, 1801–1810.
(40) Kubiak, C. P.; Woodcock, C.; Eisenberg, R. *Inorg. Chem.* **1980**, *19*, 2733–2739.
(41) Vaartstra, B. A.; O'Brien, K. N.; Eisenberg, R.; Cowie, M. *Inorg. Chem.* **1988**, *27*, 3668–3672.
(42) Oldham, S. M.; Houlis, J. F.; Sleigh, C. J.; Duckett, S. B.; Eisenberg, R. *Organometallics* **2000**, *19*, 2985–2993.
(43) Weller, A. S.; McIndoe, J. S. *Eur. J. Inorg. Chem.* **2007**, 4411–4423.
(44) Fujita, K.; Takahashi, Y.; Nakaguma, H.; Hamada, T.; Yamaguchi, R. *J. Organomet. Chem.* **2008**, *693*, 3375–3382.